IOP Publishing Journal of Physics A: Mathematical and Theoretical
J. Phys. A: Math. Theor. **47** (2014) 485002 (18pp) doi:10.1088/1751-8113/47/48/485002

Ageing and confinement in non-ergodic heterogeneous diffusion processes

Andrey G Cherstvy[1], Aleksei V Chechkin[1,2,3] and Ralf Metzler[1,4]

[1] Institute for Physics & Astronomy, University of Potsdam, D-14476 Potsdam, Germany
[2] Akhiezer Institute for Theoretical Physics, National Science Center, Kharkov Institute of Physics and Technology, Kharkov 61108, Ukraine
[3] Max-Planck Institute for the Physics of Complex Systems, Nöthnitzer Straße 38, D-01187 Dresden, Germany
[4] Physics Department, Tampere University of Technology, FI-33101 Tampere, Finland

E-mail: rmetzler@uni-potsdam.de

Received 9 September 2014, revised 6 October 2014
Accepted for publication 8 October 2014
Published 11 November 2014

Abstract

We study the effects of ageing—the time delay between initiation of the physical process at $t = 0$ and start of observation at some time $t_a > 0$—and spatial confinement on the properties of heterogeneous diffusion processes (HDPs) with deterministic power-law space-dependent diffusivities, $D(x) = D_0 |x|^\alpha$. From analysis of the ensemble and time averaged mean squared displacements and the ergodicity breaking parameter quantifying the inherent degree of irreproducibility of individual realizations of the HDP we obtain striking similarities to ageing subdiffusive continuous time random walks with scale-free waiting time distributions. We also explore how both processes can be distinguished. For confined HDPs we study the long-time saturation of the ensemble and time averaged particle displacements as well as the magnitude of the inherent scatter of time averaged displacements and contrast the outcomes to the results known for other anomalous diffusion processes under confinement.

Keywords: stochastic processes, anomalous diffusion, ageing, weak ergodicity breaking
PACS numbers: 05.40.-a., 02.50.Ey, 87.10.Mn

(Some figures may appear in colour only in the online journal)

1. Introduction

Anomalous diffusion generally refers to a stochastic process with a nonlinear time dependence of the mean squared displacement (MSD). Often, the notion of anomalous diffusion pertains to the power-law form [1–3]

$$\langle x^2(t)\rangle \simeq t^{\beta}, \tag{1}$$

where β is the anomalous diffusion exponent. For $0 < \beta < 1$ we refer to this anomalous motion as subdiffusion, for $\beta > 1$ it is superdiffusion, including the special case of ballistic motion $\beta = 2$. In the limiting case $\beta = 1$, the law (1) reduces to the linear growth in time of regular Brownian motion. There exist a number of stochastic models to describe anomalous diffusion of the form (1) [1–8]. The most relevant include continuous time random walks (CTRW) processes with scale-free distributions of waiting times [9], fractional Brownian motion [10] and the associated fractional Langevin equation motion [11], diffusion on fractal supports such as critical percolation clusters [12], as well as diffusion processes with time- [13–15] and space-dependent [15–18] diffusion coefficients. We also mention diffusion processes for which $\beta = 1$ but the associated probability density function (PDF) $P(x, t)$ is non-Gaussian [19].

The fact that different stochastic processes share the behaviour of the MSD (1) is due to the non-universal character of anomalous diffusion: the physical mechanism breaking the convergence to a Gaussian PDF $P(x, t)$ and the linear time dependence of the MSD may be different, depending on the system and/or the temporal and spatial ranges we consider. In particular, with the impressive advances in single particle tracking and other microscopic techniques as well as large scale computer simulations, it has become clear that the anomalous diffusion behaviour in physical systems indeed has different origins. In particular, CTRW type diffusion was observed for various sub-micron tracers in living biological cells [20, 21] and structured colloidal systems [22], as well as for charge carrier motion in amorphous semiconductors [9, 23]. Fractional Brownian and Langevin equation motion was shown to control the dynamics in simple membranes [24], the motion of polymers in living cells [25], and the tracer motion in complex liquids [26]. For the diffusion of smaller tracers in living biological cells, in contrast, it was found that their motion is best described by a spatially varying, local diffusion coefficient [27].

An important ingredient in the physical description of such systems are spatial confinement and ageing. Observing the motion of mobile tracers in biological cells, it becomes obvious that they multiply collide with the cell wall or other internal structures [28]. Confined diffusion is ubiquitous in the compartmentalized interior in spaces between poly-disperse obstacles in the severely crowded [29] cyto- and nucleo-plasm of eukaryotic cells [27]. Directional thermal and active transport of water molecules in the brain white matter is another example of orientation-dependent non-Brownian diffusion [30]. Concurrently, it was shown experimentally in several systems that the physical observables explicitly depend on the age of the system [20, 23].

Here we analyse both effects in the HDP model with power-law spatial dependence of the diffusion coefficient, $D(x) \simeq D_0|x|^{\alpha}$. We examine the ensemble and time averaged MSD for the HDP process as well as the degree of randomness of (long) time averages of individual realizations of the process. As we will see, the ageing effects in this system are remarkably similar to those observed in the non-stationary subdiffusive CTRW process [31, 32]. However, we point out how both processes can be distinguished. We also analyse in detail the relaxation behaviour of HDPs under confinement to a finite domain and discuss the differences to other confined anomalous diffusion processes.

We first summarize the definitions and main properties of the HDP process in section 2. We then proceed to analyse the behaviour of ageing HDPs in section 3. The confinement effects for HDPs are discussed in section 4. Finally, in section 5 we draw our conclusions and provide some additional graphs in appendix.

2. Free HDPs and their non-aged properties

Here we briefly present the main properties of free, unconfined HDPs. These are defined in terms of the stochastic Langevin equation [16]

$$\frac{\mathrm{d}x(t)}{\mathrm{d}t} = \sqrt{2D(x)}\ \zeta(t) \tag{2}$$

with the explicitly space-dependent diffusivity $D(x)$. Equation (2) is interpreted in the Stratonovich mid-point sense, that is, in this approach we use

$$x_{i+1} = x_i + \sqrt{2D\left[(x_i + x_{i+1})/2\right]}\ (y_{i+1} - y_i) \tag{3}$$

in the finite-difference displacement scheme. The increments of the Wiener process $y(t)$ represent Gaussian white noise with unit variance and zero mean, $\langle \zeta(t)\zeta(t')\rangle = \delta(t - t')$ and $\langle \zeta(t)\rangle = 0$ [16, 18], where $\delta(x)$ is the Dirac delta-function. For the diffusivity we use the following form

$$D(x) = D_0 \begin{cases} |x|^{\alpha} + \left|x_{\mathrm{off}}\right|^{\alpha}, & \alpha > 0, \\ 1\Big/\left(|x|^{-\alpha} + \left|x_{\mathrm{off}}\right|^{-\alpha}\right), & \alpha < 0, \end{cases} \tag{4}$$

such that the dimension of the coefficient D_0 is $\mathrm{cm}^{2-\alpha}\,\mathrm{s}^{-1}$. The asymptotic behaviour for $|x| \gg |x_{\mathrm{off}}|$ is the power-law

$$D(x) \sim D_0 |x|^{\alpha}. \tag{5}$$

To avoid trapping of particles for $\alpha > 0$ or divergence of $D(x)$ for $\alpha < 0$ at the position $x = 0$ in the numerical analysis below we introduced the (small) offset $x_{\mathrm{off}} = (10^{-3})^{1/\alpha}$ in equation (4). For analytical calculations in the long-time limit we neglect this offset term. The initial condition $\lim_{t\to 0} x(t) = x_0 = 10^{-1}$ is used in the simulations throughout this work. The starting point affects the MSD value of HDPs only for the initial diffusion steps. The long-time behaviour of free and confined HDPs remains unaffected. For the latter, many reflections from the walls during the simulation time t occur.

Depending on the magnitude of the scaling exponent α, the HDP with diffusivity (5) produces the MSD [16, 18, 33]

$$\langle x^2(t)\rangle = \frac{\Gamma(p + 1/2)}{\pi^{1/2}} \left(\frac{2}{p}\right)^{2p} (D_0 t)^p \tag{6}$$

with the anomalous diffusion exponent

$$p = \frac{2}{2 - \alpha}. \tag{7}$$

In particular, this relation implies that we obtain subdiffusion when $D(x)$ is a decreasing function of $|x|$, and superdiffusion is obtained when $D(x)$ is an increasing function of $|x|$. We note that previously we also considered other forms of $D(x)$ such as logarithmic and

exponential dependencies [34]. In the latter case, the resulting diffusion process is ultraslow, with Sinai-type logarithmic time dependence $\left\langle x^2(t)\right\rangle \sim \log^2(t)$ of the MSD.

Apart from the MSD (6), we are interested in the corresponding time averaged observable, the time averaged MSD [4–8]

$$\overline{\delta^2(\Delta)} = \frac{1}{T-\Delta}\int_0^{T-\Delta}(x(t+\Delta)-x(t))^2\mathrm{d}t, \tag{8}$$

in which Δ is the so-called lag time, representing the width of the window slid along the particle position time series $x(t)$, which runs in the interval $t = 0\ldots T$. We call T the measurement time of the time series $x(t)$. The time averaged MSD is the natural observable when we want to analyse individual trajectories from single particle tracking experiments or from large-scale simulations. In the following we also consider the average

$$\left\langle \overline{\delta^2(\Delta)}\right\rangle = \frac{1}{N}\sum_{i=1}^{N}\overline{\delta_i^2(\Delta)} \tag{9}$$

over N individual trajectories indexed by i. HDPs with diffusivity (5) give rise to time series $x(t)$, for which the time averaged MSD becomes

$$\left\langle \overline{\delta^2(\Delta)}\right\rangle \sim \frac{\Gamma(p+1/2)}{\pi^{1/2}}\left(\frac{2}{p}\right)^{2p}D_0^p\frac{\Delta}{T^{1-p}} = \left(\frac{\Delta}{T}\right)^{1-p}\langle x^2(\Delta)\rangle, \tag{10}$$

where in the second equality we showed the connection to the MSD (6). The fact that the time averaged MSD scales linearly and thus exhibits the distinct disparity from the MSD (6) is referred to as weak ergodicity breaking [35–37]. Measuring the time averaged MSD of the HDP in experiments could thus erroneously be interpreted as a normal diffusion process, despite the clear underlying anomalous diffusion nature exemplified in the MSD (6). One way to find out that the law (10) is indeed incompatible with normal diffusion could be to probe the dependence of $\left\langle \overline{\delta^2(\Delta)}\right\rangle$ on the measurement time T. According to equation (10) the time averaged MSD decays or grows with T depending on the value of the scaling exponent p. Physically, this corresponds to locking of the particle in regions of progressively smaller diffusivity for the subdiffusive case ($0 < p < 1$), or to the exploration of ever higher diffusivity regions for superdiffusion ($p > 1$).

3. Aged HDPs

In this section we study the effects of ageing, the dependence of a physical measurement starting at a time $t_a > 0$—the ageing time—after the initial preparation of the system at $t = 0$. Remarkably, we will see a similarity with CTRW processes with diverging characteristic waiting time.

3.1. Mean squared displacement

Consider the following situation. We initialize our system at $t = 0$ and let it evolve until time $t_a > 0$, that is, we let the system *age*. At t_a we then start to record the dynamics of the system. The ageing effect for the MSD is found easily as (compare [32])

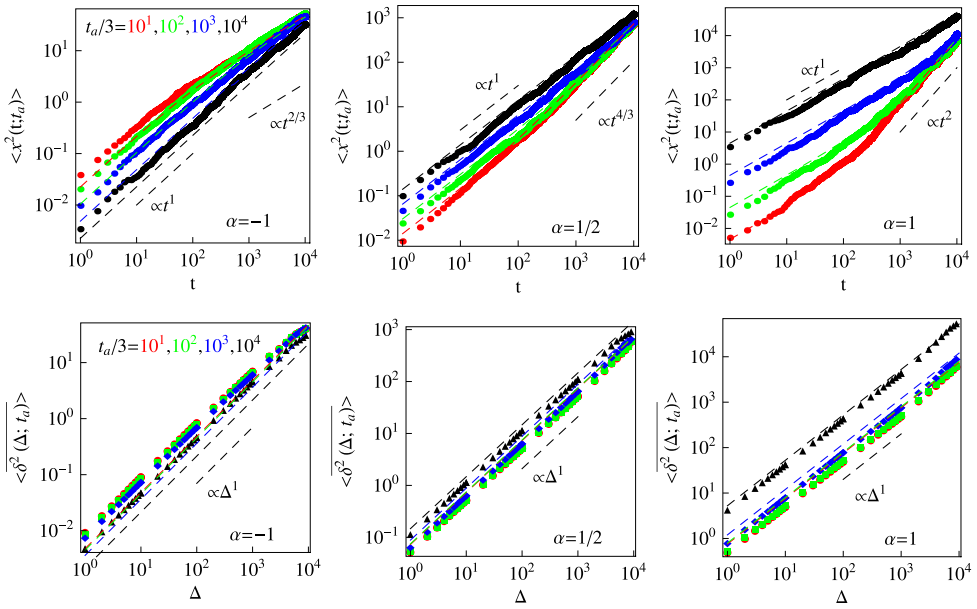

Figure 1. MSD and time averaged MSD of the aged HDPs for sub- and superdiffusive values of the scaling exponent α, as indicated in the plots. The data points with the corresponding colour correspond to different ageing times t_a. The dashed curves in the same colours represent the asymptotes (11) and (15). For the time averaged MSD 10 points per decade are shown, while for the MSD every point is shown in the plots. Parameters: $N = 500$ traces of $T = 10^5$ length were simulated.

$$\begin{aligned}\left\langle x_a^2(t_a, t)\right\rangle &= \left\langle \left[x(t_a + t) - x(t_a)\right]^2 \right\rangle \\ &= \frac{\Gamma(p + 1/2)}{\pi^{1/2}} \left(\frac{2}{p}\right)^{2p} D_0^p \left[(t_a + t)^p - t_a^p\right] \\ &\sim \frac{\Gamma(p + 1/2)}{\pi^{1/2}} \left(\frac{2}{p}\right)^{2p} D_0^p \begin{cases} t^p, & t_a \ll t \\ p t_a^{p-1} t, & t_a \gg t \end{cases},\end{aligned} \tag{11}$$

where by definition here t counts the time of the measurement, that is, the time t starts at the end of the ageing period. In analogy to the subdiffusive CTRW case [32] we thus find a crossover from the ageing dominated scaling $\langle x_a^2(t_a, t)\rangle \simeq t_a^{p-1} t$—in which the t dependence deceivingly suggests normal Brownian scaling with the time t—to the long time behaviour $\langle x_a^2(t_a, t)\rangle \simeq t^p$. Of course, when the ageing time is vanishingly small, the MSD exhibits just the regular scaling (6).

Figure 1 shows the behaviour of the aged MSD revealing good agreement with the analytical form (11). In particular, for progressively longer ageing times t_a the crossover from the ageing controlled scaling $\langle x^2(t)\rangle \simeq t$ to the anomalous scaling $\langle x^2(t)\rangle \simeq t^p$ is nicely visible. For subdiffusive HDP ($0 < p < 1$) this crossover corresponds to a decrease in the slope, while for superdiffusive HDPs ($p > 1$) the slope increases at the crossover time when t and t_a are of the same order.

What is the behaviour of the aged time averaged MSD? Following the above physical measurement scenario, we define this observable as [32]

$$\overline{\delta^2(\Delta; t_a)} = \frac{1}{T-\Delta}\int_{t_a}^{t_a+T-\Delta}(x(t+\Delta)-x(t))^2 dt, \tag{12}$$

as well as the mean over N individual trajectories,

$$\left\langle \overline{\delta^2(\Delta; t_a)} \right\rangle = \frac{1}{N}\sum_{i=1}^{N}\overline{\delta_i^2(\Delta; t_a)}. \tag{13}$$

According to our previous notation, T denotes the length of the measurement, as measured from t_a. Using the representation of the particle displacement in terms of the Wiener process $y(t) = \int_0^t \zeta(t')dt'$ in the form $x(t) \sim \sqrt{2D_0}|y(t)|^p$ such that in the appropriate limit $\Delta/T \ll 1$ we find

$$\left\langle \overline{\delta^2(\Delta; t_a)} \right\rangle \sim \frac{\Gamma(p+1/2)}{\pi^{1/2}}\left(\frac{2}{p}\right)^{2p} D_0^p\left((t_a+T)^p - t_a^p\right)\frac{\Delta}{T}. \tag{14}$$

In comparison to the non-aged result (8), the effect of the ageing enters exclusively via the expression in the parenthesis in front of the linear ratio Δ/T of lag and measurement times. For the ratio of the aged versus the non-aged time averaged MSDs

$$\Lambda_p(t_a/T) = \frac{\left\langle \overline{\delta^2(\Delta; t_a)} \right\rangle}{\left\langle \overline{\delta^2(\Delta; t_a=0)} \right\rangle} \sim (1+t_a/T)^p - (t_a/T)^p, \tag{15}$$

we thus find the simple algebraic result in full analogy with the result for the subdiffusive CTRW [32]. The ageing factor $\Lambda_p(x)$ for $0 < p < 1$ has a sigmoidal crossover from $\lim_{x\to 0}\Lambda_p(x) = 1$ in the non-aged limit to $\lim_{x\to\infty}\Lambda_p(x) = 0$ in the limit of very strong ageing. Physically, this effect emerges when during the ageing period the particles increasingly venture into areas of extremely low diffusivity and thus effectively become more and more trapped. In contrast, for superdiffusive HDPs with $p > 1$ the factor $\Lambda_p(x)$ crosses over from $\lim_{x\to 0}\Lambda_p(x) = 1$ to the scaling $\lim_{x\to\infty}\Lambda_p(x) \simeq px^{p-1}$. Here the particles find regions of ever higher diffusivity during the ageing period and with the ageing time t_a the measured time averaged MSD strongly increases.

In figure 2(a) we present the results of simulations for the ratio (15) of the aged and non-aged time averaged MSDs for HDPs. We observe that the agreement of the simulations with the predicted form (14) is particularly good for moderate values of the scaling exponent α, when the excursions of particles from the origin are not extremely fast and distant. We also observe in figure 2(a) that for a given value of t_a/T the results obtained from the time averaging over a longer trace length T are closer to the theoretical result (15), refer to the blue symbols in figure 2(a). This is statistically expected. For non-ageing Brownian motion with $\alpha = 0$ we consistently find $\Lambda_p = 1$.

We stress that it is a remarkable property of HDPs with power-law diffusivity (5) that they exhibit an identical ageing behaviour of the time averaged MSD as CTRW processes with scale-free waiting time distributions. Physically both processes are fundamentally different. HDPs are Markovian processes with a quenched distribution of diffusivities and therefore local variations of the typical times for particle jumps. In the CTRW picture the waiting times are annealed, that is, successive waiting times are fully independent, however, their mean diverges. From the results presented here we conclude that in both non-aged and aged situations measurements of the ensemble and time averaged MSDs will not allow one to distinguish between HDPs and CTRW processes. In principle, one could distinguish the two processes by inspection of the bare trajectories $x(t)$. However, these are not always available

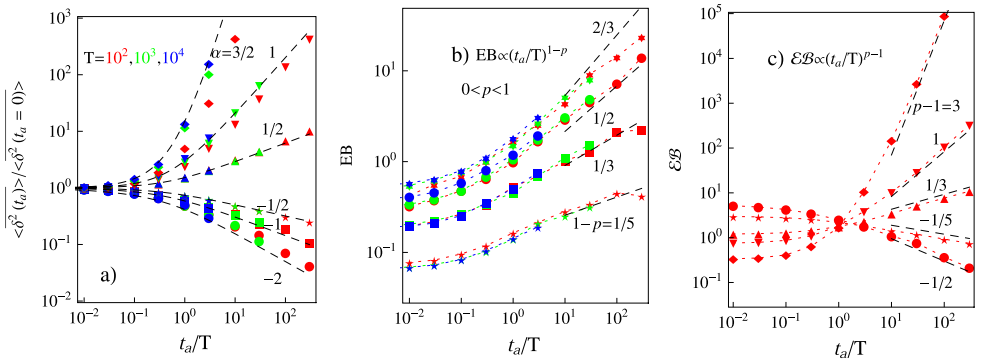

Figure 2. (a) Ratio of the aged time averaged MSD for an HDP with power-law diffusivity (5) versus the non-aged result, in the limit $\Delta/T \ll 1$, plotted for different values of the scaling exponent α. (b) Ergodicity breaking parameters EB for subdiffusive HDPs and (c) ergodic parameter $\mathcal{EB}$ plotted versus the ageing time. Note that superdiffusive HDPs do not feature the EB $\sim(t_a/T)^{1-p}$ scaling behaviour. The asymptotes of equation (15), (20), and (21) are shown as the dashed curves in panels (a), (b), and (c), respectively, for the corresponding $p = 2/(2 - \alpha)$ values. For clarity, not all α values are represented in each panel. Parameters: individual traces are in total 10^5 steps long, the trace lengths T are listed in panel (a) and correspond to different colours of the symbols. For each α value averaging over $N = 600$ trajectories was performed. The symbols for different α values have the same meaning in all three panels.

at sufficient precision and resolution to allow reliable conclusions. Moreover, additional environmental noise may further blur the local details of recorded trajectories [38].

3.2. Ergodicity breaking parameter

We now address how reproducible individual trajectories of the aged HDP process are. From subdiffusive CTRW processes, we know that, due to the divergence of the characteristic waiting time, individual time averages of physical observables remain random quantities, no matter how long the measurement time is [39]. For HDPs with power-law diffusivity the amplitude variations of the time averaged MSD also converge to a constant value, indicating the asymptotic randomness of $\overline{\delta^2}$ [16]. We analyse the exact behaviour of aged HDPs in terms of the ergodicity breaking parameter and the distribution of the amplitudes of individual time averaged MSDs.

The amplitude variation of the time averaged MSD of individual trajectories can be quantified by the PDF $\phi(\xi)$ as function of the dimensionless variable [37]

$$\xi = \frac{\overline{\delta^2(\Delta;\, t_a)}}{\left\langle \overline{\delta^2(\Delta;\, t_a)} \right\rangle}. \tag{16}$$

The variance of this distribution constitutes the ergodicity breaking parameter [37, 40]

$$\mathrm{EB} = \lim_{T/\Delta \to \infty} \left(\langle \xi^2 \rangle - 1 \right), \tag{17}$$

noting that $\langle \xi \rangle = 1$. EB = 0 is a sufficient condition for the ergodicity of a process. We also consider the alternative ergodicity parameter [41]

$$\mathcal{EB}\left(\Delta, t_{\rm a}\right) = \frac{\left\langle \overline{\delta^2\left(\Delta, t_{\rm a}\right)}\right\rangle}{\left\langle x^2\left(\Delta; t_{\rm a}\right)\right\rangle}, \tag{18}$$

which is to be equal unity to represent a necessary condition for ergodicity. Without ageing, the ergodicity breaking parameter EB for HDPs decreases with growing anomalous diffusion exponent p and then increases again for superdiffusive values [16].

For subdiffusive CTRWs with $0 < \beta < 1$, EB $= 2\Gamma^2(1+\beta)/\Gamma(1+2\beta) - 1$ monotonically decreases from unity to zero when β is varied from zero to unity for long measurement times [37]. For Brownian motion the decay of the ergodicity breaking parameter follows [42]

$$\mathrm{EB}(\Delta) \sim \frac{4\Delta}{3T} \tag{19}$$

in the limit $\Delta/T \to 0$. Brownian motion has stationary increments and therefore the process is independent of ageing. Therefore, the scaling (19) is preserved for any $t_{\rm a}$. For CTRW processes it was found that the ergodicity breaking parameter for any finite but sufficiently long T scales like $\mathrm{EB}(t_{\rm a}) \sim 2(t_{\rm a}/T)^{1-\beta}/[\beta(1+\beta)]$ in the limit of strong ageing, $t_{\rm a} \gg T$ [32]. As shown in figure 2(b), we observe from numerical analysis that for subdiffusive HDPs with $0 < p < 1$ (or $\alpha < 0$) the EB parameter follows the same asymptotic behaviour as subdiffusive CTRWs. In particular for moderate α, for long ageing times we find

$$\mathrm{EB}(t_{\rm a}) \simeq \left(\frac{t_{\rm a}}{T}\right)^{1-p}. \tag{20}$$

In analogy to the CTRW process [32], the divergence of the ergodicity breaking parameter in the subdiffusive regime of HDPs with $t_{\rm a}/T$ is stronger for smaller values of the anomalous diffusion exponent p, that is, when the exponent α in equation (5) assumes more negative values.

For completeness, we also present numerical results for the alternative ergodicity parameter $\mathcal{EB}$ as function of $t_{\rm a}/T$ in figure 2(c). We find that $\mathcal{EB}$ reveals much larger variations for different time averages corresponding to the same $t_{\rm a}/T$ values (not shown for clarity in figure 2(c)), as compared to the parameter EB. The ergodicity breaking parameter EB for subdiffusive HDPs is rather insensitive to the variations of $t_{\rm a}$ and T provided $t_{\rm a}/T =$ const. In contrast to Λ_p and EB, the alternative ergodicity parameter $\mathcal{EB}$ does *not* collapse onto a universal curve for the same ratio $t_{\rm a}/T$ but different $t_{\rm a}$ and T values computed along the trace (results not shown). We observe that at long ageing times the scaling law

$$\mathcal{EB} \simeq \left(\frac{t_{\rm a}}{T}\right)^{p-1} \tag{21}$$

is valid. Asymptotes (20) and (21) are shown as the dashed lines in figures 2(b) and (c), respectively.

We complement the study of the parameter EB with the analysis of the distribution of individual $\overline{\delta^2(\Delta; t_{\rm a})}$ traces of aged HDPs. For the lag time $\Delta = 1$ this distribution is illustrated in figure 3. We observe that for longer ageing times $t_{\rm a}$ subdiffusive particles with $\alpha < 0$ become increasingly localized and therefore the amplitude of the $\overline{\delta^2}$ traces are shifted towards smaller values. When $\alpha > 0$, corresponding to superdiffusion, the spread of $\overline{\delta^2}$ grows and distant particle excursions produce large amplitudes of the time averaged MSD. For both sub- and superdiffusive aged HDPs the distributions of the time averaged MSD $\overline{\delta^2}$ approach zero at small $\overline{\delta^2}$ values. In other words, no trajectory exists, in which the particle is fully immobile.

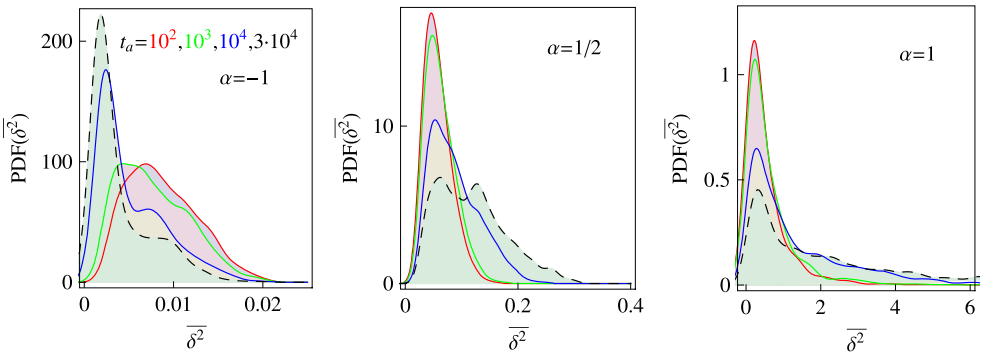

Figure 3. Amplitude scatter of the time averaged MSD of individual trajectories, shown at lag time $\Delta = 1$. The shown results are computed for the trace length $T = 10^4$ and the indicated ageing times t_a. The other parameters are the same as in figure 2. Note that the curves reach zero for vanishing values of the time averaged MSD. Also note the different scales for the magnitudes of time averaged MSDs. The somewhat bumpy structure in the scatter PDF of the time averaged MSD traces is mainly because of a finite number of traces ($N = 900$ for this figure). This becomes particularly visible for the longest ageing time t_a when the statistics of the distribution is insufficient, due to computational limitations.

This finding is in contrast to subdiffusive CTRWs, in which a finite fraction of immobile walkers always exists [32].

A useful parameter to classify stochastic processes is the non-Gaussianity parameter. In one dimension it is defined in terms of time averaged quantities through [7, 43]

$$G\left(\Delta; t_a\right) = \frac{\left\langle \overline{\delta^4\left(\Delta, t_a\right)} \right\rangle}{3\left\langle \overline{\delta^2\left(\Delta, t_a\right)} \right\rangle^2} - 1, \tag{22}$$

where the fourth time averaged moment is given by

$$\overline{\delta^4\left(\Delta; t_a\right)} = \frac{1}{T-\Delta}\int_{t_a}^{t_a+T-\Delta} \left(x(t+\Delta) - x(t)\right)^4 \mathrm{d}t. \tag{23}$$

The non-Gaussianity parameter for aged *subdiffusive* HDPs shows a similar scaling with t_a/T as the EB parameter, as we demonstrate in figure A.1. Overall, the magnitude of the parameter G is small for moderate values of $|\alpha|$ and progressively increases for more pronounced sub- or superdiffusive HDPs, in line with the results for $G(\alpha)$ for non-aged HDPs [18]. The trends of increasing G for stronger superdiffusive HDPs is similar to our observations for the EB parameter (results not shown).

4. Confined HDPs

We now turn to the effects of spatial confinement by hard reflective walls on HDPs with power-law diffusivity (5). In particular, we address their ergodic behaviour under these boundary conditions. In this section, no ageing is considered.

4.1. Mean squared displacement

In our simulations we implement reflecting boundary conditions on the particles to study the confined dynamics in the domain $-L < x < L$. We observe in the resulting figure 4 that for large values of the scaling exponent α of the diffusivity (5) the reflecting boundary is reached after a smaller number of steps and thus the MSD and time averaged MSD start to saturate earlier. In the long-time limit $t \to \infty$ we find the relaxation $\left\langle \overline{\delta^2} \right\rangle \simeq \Delta^0$ to a plateau. Due to definition (8) the time averaged MSD amounts to *twice* the value for the MSD. The latter saturates at the α-dependent stationary plateau

$$\left\langle x^2 \right\rangle_{\rm st} = \frac{1}{2} \left\langle \overline{\delta^2} \right\rangle_{\rm st} \approx p^{-\nu} \frac{L^2}{3} \tag{24}$$

with $\nu \approx 0.6$, as extracted from fitting the values $\langle x^2 \rangle_{\rm st}$ of the plateaus in figure A.2 . This result includes the correct limiting value for confined Brownian motion when $\alpha = 0$ and $p = 1$ corresponding to the uniform distribution $p(x) = 1/(2L)$ for Brownian motion. For confined HDPs the PDFs are not uniform in the confined domain, see below, and therefore the stationary value $\langle x^2 \rangle_{\rm st}$ explicitly depends on the value of the anomalous diffusion exponent p. At the end of the time trace at $\Delta \to T$ the definition (8) features a pole, effecting that the time averaged MSD converges to the MSD, $\langle x^2(T) \rangle \to \langle \overline{\delta^2(T)} \rangle$. This drop in the traces $\langle \overline{\delta^2(t \to T)} \rangle$ is more pronounced for shorter traces and smaller $|\alpha|$ values. To see this, for the green portions of the curves in figure 4(a) fine linear grid is used, rather than the log-sampling with ten points per decade as for the remainder of the shown curves, see figures 4 and A.3 .

These features of the MSD and the time averaged MSD are similar to those of confined Brownian and fractional Brownian motion [4, 8, 44, 45]. However, for fractional Brownian motion confined in an harmonic potential the dependence of the stationary value of the MSD is $\langle x^2 \rangle_{\rm st} \simeq \Gamma(1 + \alpha)$ [46]. Note that when an harmonic potential confines the particle rather than hard walls, the onset of the saturation in the MSD will appear earlier. We also note that, as shown in figure 4, initially the time averaged MSD grows linearly in the lag time Δ, before reaching the saturation. Having started right next to the origin, the particle first performs free HDP motion given by equation (10). This linear behaviour for $\langle \overline{\delta^2} \rangle$ is indicated by the dot-dashed lines in figure 4. The magnitude of $\langle \overline{\delta^2} \rangle$ for confined HDPs shown here varies only slightly with α, in contrast to asymptotically free HDPs (see figure 2 in [18]).

We note that in contrast to the convergence to the α-dependent plateau (24) for HDPs, the MSD of confined subdiffusive CTRW processes converges to the thermal value $\langle x^2 \rangle_{\rm st} = L^2/3$ [47]. The time averaged MSD of CTRWs *does not* exhibit a convergence to a plateau at all but continues to grow in confinement, with the shallower power-law $\left\langle \overline{\delta^2(\Delta)} \right\rangle \sim (\Delta/T)^{1-\beta}$ at longer lag times [39, 48]. The pre-factor of this scaling law is given by the first two moments of the associated Boltzmann equilibrium distribution [4, 39].

Due to the confinement imposed onto the motion, the amplitude variations of individual time averaged MSD $\overline{\delta^2}$ is much smaller than for free HDPs with the same α. This effect is particularly dramatic for strongly superdiffusive HDPs, compare figure 4 with the corresponding panels in figure 2 of [18]. This strong change of the width of the amplitude scatter $\phi\left(\overline{\delta^2} / \langle \overline{\delta^2} \rangle \right)$ is in stark contrast to the scatter of confined CTRWs [4, 8, 39]. In the latter process the amplitude variations solely stems from the statistics of the number of jumps performed by the particle [32]. The scatter we get for confined HDPs is comparable to that of ordinary Brownian motion with the same length T of the time traces. For progressively weaker confinement, that is, larger L values, the amplitude scatter of the $\overline{\delta^2}$ traces grows and

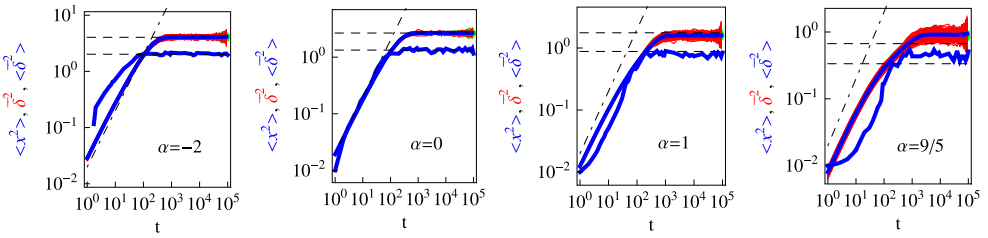

Figure 4. Time evolution of the MSD (thick blue curves) and the time averaged MSD represented by individual time traces (thin red curves) as well as the average over many trajectories (thick blue curves) for confined HDPs with varying scaling exponent α of the diffusivity (5). We observe a distinct convergence to plateaus, whose value given by equation (24) for the corresponding α values are represented by the dashed lines. The linear asymptote of the unconfined motion is shown by the dot–dashed line to indicated the relative shift of the time averaged MSD of confined HDPs. Parameters: for each α we show $N = 300$ traces of $T = 10^5$ steps confined to the interval $x \in \{-2, 2\}$ and $x_0 = 0.1$. Log-sampling of data-points along the Δa-axis is performed for the red and blue traces. To resolve the drop of $\left\langle \overline{\delta^2} \right\rangle$ at $t \to T$, a finer $\delta\Delta = 100$ grid is used for the final portions of the $\overline{\delta^2}$ traces (green curves). For each α the computation for the T and N values used here consume about 2.5 days on a standard workstation.

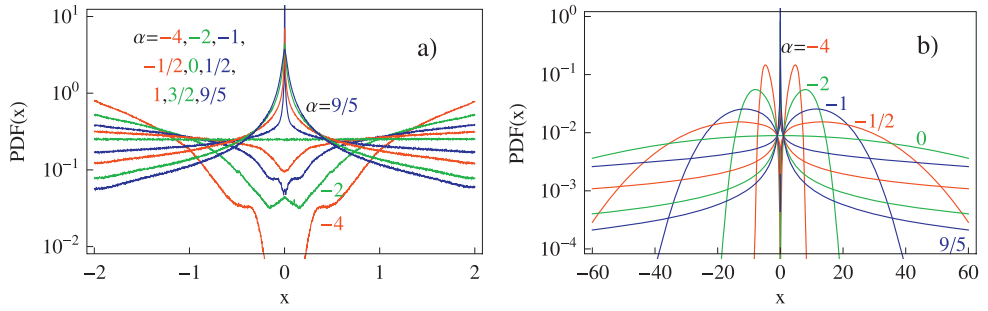

Figure 5. Probability density function of diffusing particles obtained from simulations of confined HDPs (a) and the analytical solution of non-confined HDPs [16] (b). Parameters are the same as in figure 4: $L = 2$, $T = 10^5$, $N = 300$, and the exponents α are indicated in the panels.

the magnitude of $\langle \overline{\delta^2} \rangle$ starts to approach that for the corresponding free HDPs, as shown in figure A.3. The reduction of the amplitude scatter under confinement is also observed near the critical point $\alpha \to 2$, for which unconfined HDPs reveal an extreme spread of $\overline{\delta^2}$ [18]. For decreasing length of the trajectories T, consistently the amplitude scatter $\overline{\delta^2}$ becomes substantially larger, see figure A.3.

Under confinement we observe that in the subdiffusive case with $\alpha < 0$ the value of the PDF increases when we approach the confining walls, as the particles are 'pushed' towards regions of ever smaller diffusivity, i.e., away from the origin $x = 0$, see figure 5(a). That is, the space-dependence of the diffusivity $D(x)$ acts like an effective potential on the particle. At small x values for more pronounced subdiffusive HDPs an interesting tradeoff between the

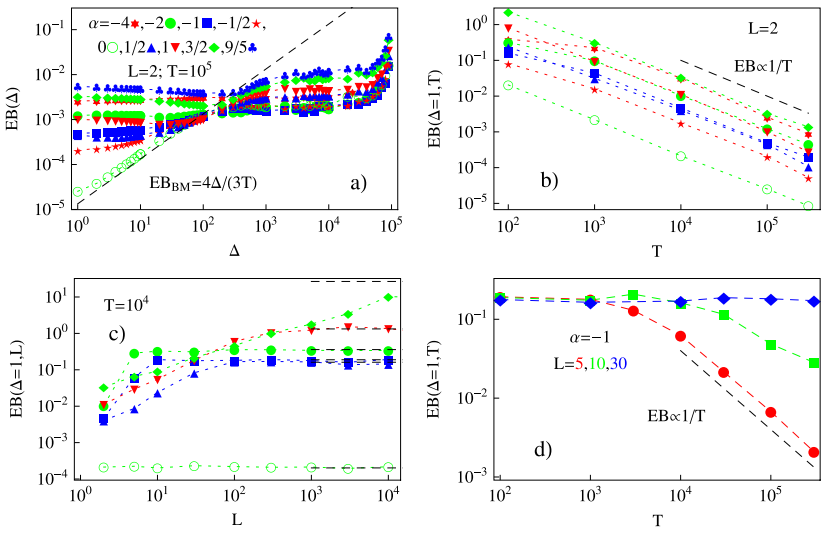

Figure 6. Ergodicity breaking parameter EB as function of the lag time Δ (a) for fixed measurement time T, (b) as function of the length T of individual trajectories for $\Delta = 1$, (c) as function of the length L of the confining interval for $\Delta = 1$, and (d) as function of the length T of individual trajectories for $\Delta = 1$ at varying extent of confinement. The symbols are the same as in figure 2, and the colour scheme is the same as in figure 5. Moreover, the colour scheme in panels (a), (b), and (c) is the same. Empty circles denote the limiting case of Brownian motion in all the panels. In panel (c) the asymptotes for $L \to \infty$ with the corresponding colour denote EB for unconfined motion [18]. At least $N = 300$ traces were used for averaging in each panel, except for the longest $T = 3 \times 10^5$ traces with only $N = 30$ trajectories generated.

depletion at the origin and the effect of the effective potential of the diffusivity are observed, leading to the relatively sharp changes of the slope, in particular, for the lowest red curve in figure 5(a) for $\alpha = -4$. In the Brownian limit the PDF is completely uniform, $p(x) = 1/(2L)$, see the green curve in figure 5(a). We find that the numerical integration of simulated PDF profiles yields a good agreement with the model prediction (24) for the MSD plateau heights, see figure A.2. For comparison, in figure 5(b) we present the PDFs of unconfined HDPs with the same α values. For the latter the bimodal character of the PDF near the origin and the complete depletion at $x = 0$ for subdiffusive HDPs the PDF is distinct, while for super-diffusive non-confined HDPs we find a cusp at $x = 0$ [16].

4.2. Ergodicity breaking parameter

We complete our study of confinement effects in HDPs with the analysis of the ergodicity breaking parameter. As shown in figure 6(a), we naturally observe that for confined HDPs the ergodicity breaking parameter EB significantly deviates from the asymptote (19) for Brownian motion. In contrast, for confined Brownian motion ($\alpha = 0$) before the walkers start to feel the reflecting walls, equation (19) is valid, see the open green symbols in figure 6(a). At moderate diffusion times, the ergodicity breaking parameter of confined Brownian motion assumes values similar to those of confined HDPs, the latter depending only weakly on α. The general form of EB for HDPs is qualitatively similar to that of confined fractional Brownian motion, see figure 9 in [44]. The discrepancy of EB of confined HDPs from the Brownian

behaviour underlines that the quenched nature of the HDP process continues to influence the (anomalous) particle motion even when the MSD reaches its plateau.

The dependence of the ergodicity breaking parameter EB in the limit $\Delta/T \to 0$ on the measurement time T is shown in figure 6(b). Remarkably, EB at $\Delta = 1$ for confined HDPs exhibits the very systematic scaling

$$\lim_{T\to\infty} \mathrm{EB} \sim 1/T \tag{25}$$

for all α values studied in simulations. This scaling is identical to the approach to ergodicity of unconfined Brownian motion, equation (19). The $1/T$ scaling obtained here for confined HDPs is reminiscent of that demonstrated for confined fractional Brownian motion, see figure 4 in [44]. Some deviations of EB from the asymptote (25) for shorter traces are due to a limited number of particle reflections from the confining walls.

We checked that the scaling $\lim_{\Delta/T\to 0} \mathrm{EB} \sim 1/T$ remains valid for other sizes of the confining box L. Clearly, for more distant positions of the reflecting boundaries equation (25) starts to be obeyed for longer traces T, see figure 6(d). The amplitude variations of the time averaged MSD traces grow for shorter T, thereby effecting a stronger non-ergodic behaviour reflected by larger values of EB as T decreases, see figure 6(b). Also, corroborating the results for non-confined HDPs, the value of EB at $\Delta = 1$ grows from the asymptote (19) for Brownian motion as $|\alpha|$ increases and the trajectory-to-trajectory fluctuations become more pronounced. We checked that the alternative ergodic parameter reaches the value $\mathcal{EB} \to 2$ in the long time limit, as it should according to equations (18) and (24).

From simulations of HDPs confined to intervals of increasing size L we find that the ergodicity breaking parameter EB approaches the unconfined values for the respective α, as computed in [18], see figure 6(c). For larger confining boxes the value of EB at $\Delta = 1$ starts to saturate at the α-dependent crossover length $L^\star$ to the values of the corresponding free HDP, as shown in figure 6(c). The EB values at $L \to \infty$ vary strongly with the scaling exponent α, see figures 3, 4 of [18] for details. For strongly subdiffusive exponents, such as $\alpha = -2$ in figure 6(c), EB saturates to the unconfined value already after relatively short simulations intervals. In contrast, for strongly super-diffusive values such as $\alpha = 3/2$, when EB reaches large values, the unconfined behaviour is reached only for $L^\star \sim 10^{4\ldots5}$ due to contributions of extremely distant particle excursions. Note that for larger confining boxes, a greater number of traces is to be simulated to obtain the correct convergence of the ergodicity breaking parameter to the corresponding values in absence of confinement.

We also detect that the non-Gaussianity $G(\Delta)$ grows with α for relatively short lag times, while for larger Δ it attains some stationary scaling-exponent dependent values, as demonstrated in figure A.4 (a). The evolution of the auxiliary ergodic parameter for confined HDPs is presented in figure A.4(b).

5. Conclusions

We studied theoretically and by numerical integration of the stochastic Langevin equation the behaviour of HDPs in the presence of ageing and confinement, revealing a number of novel effects. Specifically we showed that for aged HDPs the properties of both the ensemble and time averaged MSDs as well as their weakly non-ergodic behaviour are strikingly similar to that of aged CTRWs when their anomalous diffusion exponent is the same. Thus, the amplitude of the aged time averaged MSD follows relation (15), while the

ergodicity breaking parameter follows the scaling (20). Based on these quantities, it is practically impossible to distinguish both processes from each other in the analysis of a given set of sample trajectories $x(t)$. However, we showed that the distribution of the amplitude scatter of the time averaged MSD between individual trajectories is fundamentally different for both processes: for HDPs it decays to zero for vanishing amplitude of the time averaged MSD, while for CTRW processes the scatter distribution remains finite at this point [49].

Our study of aged HDPs is inspired by CTRW ageing theory [32]. During the ageing period of an HDP more and more particles become localized in regions of low diffusivity. This localization is more efficient for larger values of the scaling exponent α. For CTRWs the increase of the immobilization of particles during the ageing period is due to the emergence of longer and longer waiting times, leading to a population splitting between a mobile and immobile fraction of particles [32]. Despite the quite different physical details between the annealed CTRW process and the quenched HDP, the fact that the power-law distribution of diffusivities can be translated into a power-law distribution of local jump times effectively leads to the similar behaviour of the two processes. As said, however, this similarity breaks when we consider the statistics of the amplitude distribution of individual time averaged MSD traces.

Confined HDPs show a drastically different behaviour in comparison to confined CTRWs. While the time averaged MSD for the latter continues to grow as power-law of the lag time, the same quantity for HDPs converge to a plateau. This convergence is similar to the behaviour of fractional Brownian motion. The dependence of the plateau values on the anomalous diffusion exponent of both processes is different. Purely from the analysis of the ensemble and time averaged MSDs for a given system with fixed anomalous diffusion exponent, however, it will again be practically impossible to distinguish the two processes. Other, complementary quantities, need to be evaluated, compare the studies in [50]. Concurrently to the convergence of the MSD to a plateau, for confined HDPs the impediment of distant particle excursions gives rise to a dramatically reduced spread of the amplitude of the time averaged MSD.

As modern experimental techniques provide an increasing number of long single particle trajectories at unprecedented resolution, and anomalous diffusion becomes recognized as a widely spread phenomenon [8], the need for more detailed stochastic models and their understanding arises. We believe that this study contributes to an emerging, more complete picture of anomalous diffusion processes.

Acknowledgments

The authors acknowledge funding from the Deutsche Forschungsgemeinschaft (DFG Grant CH 707/5-1 to AGC), the Berlin Mathematical Society (grant to AVC), and the Academy of Finland (Suomen Akatemia, FiDiPro scheme to RM).

Appendix. Additional figures

Here we present some additional figures for reference in the main text.

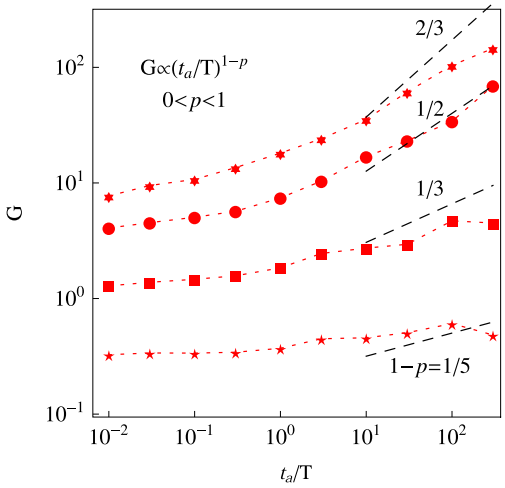

Figure A1. Non-Gaussianity parameter (22) for subdiffusive HDPs as function of the ageing time t_a computed for $T = 10^2$. The parameters used, the notations for the symbols, and the scaling asymptotes shown are the same as in figure 2(b).

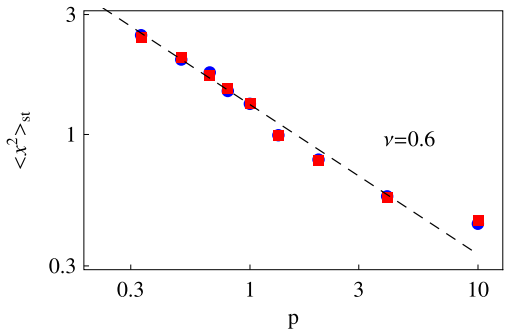

Figure A2. Plateau MSD stationary values, as predicted by equation (24) (the dashed curve), obtained from numerical integration of the PDF profiles in figure 5(a) (red symbols) and by direct fit of the later fragments of the averaged time averaged MSD curves in figure 4 (blue symbols). Parameters: $T = 10^5$, $L = 2$.

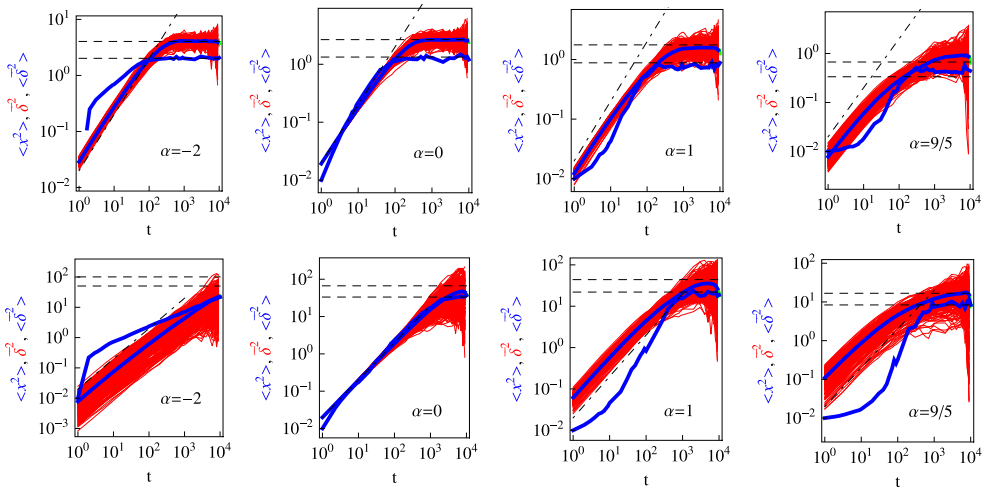

Figure A3. The same as in figure 4 but for shorter traces $T = 10^4$ confined to the intervals with $L = 2$ (top panel) and $L = 10$ (bottom panel).

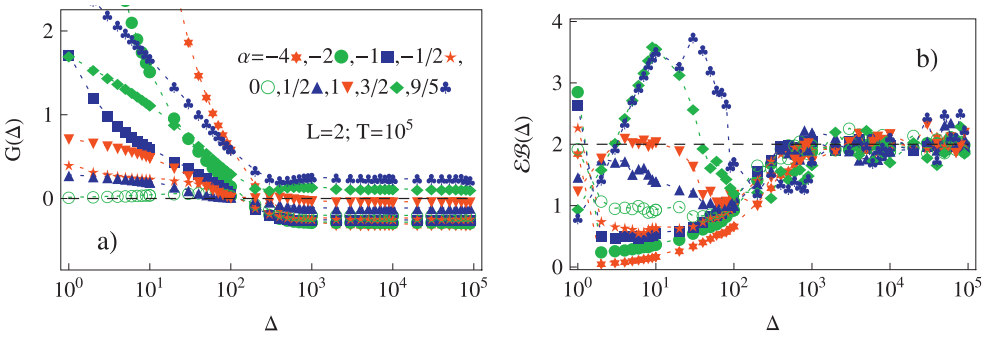

Figure A4. The dependence of $G(\Delta)$ and $\mathcal{EB}(\Delta)$ for confined HDPs. Parameters and symbol notations are the same as in figure 6(a).

References

[1] Bouchaud J-P and Georges A 1990 *Phys. Rep.* **195** 127
[2] Hughes B D 1995 *Random Walks and Random Environments* vol 1 (Oxford: Oxford University Press)
[3] Metzler R and Klafter J 2000 *Phys. Rep.* **339** 1
Metzler R and Klafter J 2004 *J. Phys. A: Math. Gen.* **37** R161
[4] Burov S, Jeon J-H, Metzler R and Barkai E 2011 *Phys. Chem. Chem. Phys.* **13** 1800
[5] Sokolov I M 2012 *Soft Matter* **8** 9043
[6] Barkai E, Garini Y and Metzler R 2012 *Phys. Today* **65** 29
[7] Höfling F and Franosch T 2013 *Rep. Prog. Phys.* **76** 046602
[8] Metzler R, Jeon J-H, Cherstvy A G and Barkai E 2014 *Phys. Chem. Chem. Phys.* at press (doi:10.1039/C4CP03465A)
[9] Scher H and Montroll E W 1975 *Phys. Rev.* B **12** 2455
[10] Mandelbrot B B and van Ness J W 1968 *SIAM Rev.* **10** 422
Kolmogorov A N 1940 *Dokl. Akad. Nauk SSSR* **26** 6

[11] Lutz E 2001 *Phys. Rev.* E **64** 051106
Goychuk I 2009 *Phys. Rev.* E **80** 046125
Goychuk I 2012 *Adv. Chem. Phys.* **150** 187
[12] Havlin S and Ben-Avraham D 1987 *Adv. Phys.* **36** 695
[13] Lim S C and Muniandy S V 2002 *Phys. Rev.* E **66** 021114
Thiel F and Sokolov I M 2014 *Phys. Rev.* E **89** 012115
[14] Jeon J-H, Chechkin A V and Metzler R 2014 *Phys. Chem. Chem. Phys.* **16** 15811
[15] Fuliński A 2013 *J. Chem. Phys.* **138** 021101
Fuliński A 2011 *Phys. Rev.* E **83** 061140
[16] Cherstvy A G, Chechkin A V and Metzler R 2013 *New J. Phys.* **15** 083039
[17] Massignan P *et al* 2014 *Phys. Rev. Lett.* **112** 150603
[18] Cherstvy A G and Metzler R 2014 *Phys. Rev.* E **90** 012134
[19] Guan J, Wang B and Granick S 2014 *ACS Nano* **8** 3331
Wang B, Kuo J, Bae S C and Granick S 2012 *Nat. Mater.* **11** 481
[20] Tabei S M A, Burov S, Kim H Y, Kuznetsov A, Huynh T, Jureller J, Philipson L H, Dinner A R and Scherer N F 2013 *Proc. Natl Acad. Sci. USA* **110** 4911
Weigel A V, Simon B, Tamkun M M and Krapf D 2011 *Proc. Natl Acad. Sci. USA* **108** 6438
[21] Jeon J-H, Tejedor V, Burov S, Barkai E, Selhuber-Unkel C, Berg-Sørensen K, Oddershede L and Metzler R 2011 *Phys. Rev. Lett.* **106** 048103
[22] Wong I Y, Gardel M L, Reichman D R, Weeks E R, Valentine M T, Bausch A R and Weitz D A 2004 *Phys. Rev. Lett.* **92** 178101
Xu Q, Feng L, Sha R, Seeman N C and Chaikin P M 2011 *Phys. Rev. Lett.* **106** 228102
[23] Schubert M, Preis E, Blakesley J C, Pingel P, Scherf U and Neher D 2013 *Phys. Rev.* B **87** 024203
[24] Jeon J-H, Martinez-Seara Monne H, Javanainen M and Metzler R 2012 *Phys. Rev. Lett.* **109** 188103
Kneller G R, Baczynski K and Pasienkewicz-Gierula M 2011 *J. Chem. Phys.* **135** 141105
[25] Kepten E, Bronshtein I and Garini Y 2013 *Phys. Rev.* E **87** 052713
[26] Szymanski J and Weiss M 2009 *Phys. Rev. Lett.* **103** 038102
Jeon J-H, Leijnse N, Oddershede L B and Metzler R 2013 *New J. Phys.* **15** 045011
[27] Kühn T, Ihalainen T O, Hyväluoma J, Dross N, Willman S F, Langowski J, Vihinen-Ranta M and Timonen J 2011 *PLoS One* **6** e22962
[28] Golding I and Cox E C 2006 *Phys. Rev. Lett.* **96** 098102
[29] Zhou H X, Rivas G and Minton A P 2008 *Annu. Rev. Biophys.* **37** 375
[30] le Bihan D 2003 *Nat. Rev. Neurosci.* **4** 469
[31] Monthus C and Bouchaud J-P 1996 *J. Phys. A: Math. Gen.* **29** 3847
Barkai E 2003 *Phys. Rev. Lett.* **90** 104101
[32] Schulz J H P, Barkai E and Metzler R 2013 *Phys. Rev. Lett.* **110** 020602
Schulz J H P, Barkai E and Metzler R 2014 *Phys. Rev.* X **4** 011028
[33] Cherstvy A G, Chechkin A V and Metzler R 2014 *Soft Matter* **10** 1591
[34] Cherstvy A G and Metzler R 2013 *Phys. Chem. Chem. Phys.* **15** 20220
[35] Bouchaud J-P 1992 *J. Phys. (Paris)* I **2** 1705
Bel G and Barkai E 2005 *Phys. Rev. Lett.* **94** 240602
Bel G and Barkai E 2006 *Phys. Rev.* E **73** 016125
Rebenshtok A and Barkai E 2007 *Phys. Rev. Lett.* **99** 210601
Lomholt M A, Zaid I M and Metzler R 2007 *Phys. Rev. Lett.* **98** 200603
Aquino G, Grigolini P and West B J 2007 *Europhys. Lett.* **80** 10002
Khoury M, Lacasta A M, Sancho J M and Lindenberg K 2011 *Phys. Rev. Lett.* **106** 090602
Skaug M J, Lacasta A M, Ramirez-Piscina L, Sancho J M, Lindenberg K and Schwartz D K 2014 *Soft Matter* **10** 753
[36] Lubelski A, Sokolov I M and Klafter J 2008 *Phys. Rev. Lett.* **100** 250602
Sokolov I M, Heinsalu E, Hänggi P and Goychuk I 2010 *Europhys. Lett.* **86** 30009
[37] He Y, Burov S, Metzler R and Barkai E 2008 *Phys. Rev. Lett.* **101** 058101
[38] Jeon J-H, Barkai E and Metzler R 2013 *J. Chem. Phys.* **139** 121916
[39] Burov S, Metzler R and Barkai E 2010 *Proc. Natl Acad. Sci. USA* **107** 13228
[40] Rytov S M, Kravtsov Yu A and Tatarskii V I 1987 *Principles of Statistical Radiophysics 1: Elements of Random Process Theory* (Heidelberg: Springer)
[41] Godec A and Metzler R 2013 *Phys. Rev. Lett.* **110** 020603
[42] Deng W and Barkai E 2009 *Phys. Rev.* E **79** 011112

[43] Ernst D, Kohler J and Weiss M 2014 *Phys. Chem. Chem. Phys.* **16** 7686
[44] Jeon J-H and Metzler R 2010 *Phys. Rev.* E **81** 021103
[45] Jeon J-H and Metzler R 2012 *Phys. Rev.* E **85** 021147
[46] Sliusarenko O Yu, Gonchar V Yu, Chechkin A V, Sokolov I M and Metzler R 2010 *Phys. Rev.* E **81** 041119
[47] Metzler R and Klafter J 2000 *Physica* A **278** 107
[48] Neusius T, Sokolov I M and Smith J C 2009 *Phys. Rev.* E **80** 011109
[49] Jeon J-H and Metzler R 2010 *J. Phys. A: Math. Theor.* **43** 252001
[50] Tejedor V, Bénichou O, Voituriez R, Jungmann R, Simmel F, Selhuber-Unkel C, Oddershede L and Metzler R 2010 *Biophys. J.* **98** 1364
Albers T and Radons G 2013 *Europhys. Lett.* **102** 40006
Berezhkovsky A M, Dagdug L and Bezrukov S M 2014 *Biophys. J.* **106** L09
Robson A, Burrage K and Leake M C 2012 *Phil. Trans. R. Soc.* B **368** 0029
Condamin S, Tejedor V, Voituriez R, Benichou O and Klafter J 2008 *Proc. Natl Acad. Sci. USA* **105** 5675